Dynamics of dielectric breakdown paths

Jeffrey Boksiner* and P. L. Leath†
Department of Physics and Astronomy, Rutgers, the State University of New Jersey, 136 Frelinghuysen Road, Piscataway, New Jersey 08854-8019, USA
(Received 10 February 2003; published 27 June 2003)

We investigate the dynamics and geometry of dielectric breakdown paths of needle defects of arbitrary residual resistivity in an otherwise homogeneous medium using a time-dependent electrical-circuit model. The circuit model consists of a semi-infinite lattice of capacitors in parallel with resistors that break down to a lower (residual) resistance. The breakdown occurs if the local field across a resistor exceeds a critical value for a breakdown delay time. We consider cases where the initial resistance is infinite or finite and where the residual resistance is finite or zero. We consider the model for the case where the applied field reaches the critical value adiabatically. We find that, as in the quasistatic case, the breakdown grows either one dimensionally or spreads with a fractal dimension (bifurcates) depending on the values of residual resistance and breakdown delay time. Also, we find that the propagation velocity of the needle oscillates spontaneously. We give the phase diagram for bifurcation and oscillations. We derive a simplified recursive map approximation to explain this behavior.

DOI: 10.1103/PhysRevE.67.066610 PACS number(s): 77.22.Jp, 51.50.+v, 62.20.Mk

I. INTRODUCTION

Nonlinear resistor and fuse networks provide realistic and tractable models for understanding the geometry and stability of dielectric breakdown and other breakdown phenomena [1,2]. The random-fuse network and an equivalent problem in two dimensions, namely, the random nonlinear resistor network have been studied extensively [3–7]. The random non-linear resistor model has been proposed as one of the models for dielectric breakdown [8]. Subsequent investigations have explored various features of this model, including a complete description of phase behavior and breakdown paths where the broken bonds have nonzero resistivity (residual resistivity) [5,9]. There is a thorough review of various breakdown models in Ref. [10].

The majority of the breakdown models are quasistatic. The review of Ref. [10] describes the available dynamic models. However, there have been a few studies that investigated the evolution of random-resistor networks with time-varying fields. Since the dielectric breakdown of real materials necessarily results in time-dependent fields as the breakdown progresses, it is important to understand the conditions where the previous quasistatic models are appropriate and where the time-dependence leads to important effects that are not observed in the quasistatic model.

In this paper, we study breakdown with a time-dependent evolution of the local electric field. Previous works with breakdown in homogeneous or disordered media have shown that for samples with dilute defects, the breakdown process begins at a critical defect in the network. The critical defect for dielectric breakdown is often a long, thin defect—a needle directed along the applied electric field. Characteristics of the breakdown process on a random lattice, including the breakdown field and the geometry of the breakdown cluster or the evolution of the breakdown path, often reflect the characteristics of the breakdown for a needle defect.

We are interested in understanding the evolution of the field, the oscillations that appear spontaneously, and the breakdown path as a function of the time constants and the residual resistivity. We examine the geometrical structure of the breakdown cluster in order to separate the aspects of the structure inherent in the growth of needles in homogeneous media from those arising from random disorder in systems. To perform our study, we have extended an algorithm, originally developed for the quasistatic problem, described in Appendix A, that uses Green's functions to compute the time-dependent field due to a collection of defects in an infinite homogeneous medium exactly.

A. Breakdown model

Our simulation of the breakdown growth is a direct dynamical extension of the quasistatic random-resistor breakdown model [9]. We assume that defects cause variations in material conductivity σ in an otherwise homogeneous material. The dynamical model is based on an electrical-circuit representation of the low-frequency limit of Maxwell equations where inductive terms are neglected. The material parameters are represented by the constitutive relations

$$\mathbf{D}=\epsilon\mathbf{E}, \tag{1a}$$

$$\mathbf{J}=\sigma\mathbf{E}. \tag{1b}$$

Here, the conductivity σ and the dielectric constant ϵ are considered independent of frequency. From Maxwell equations and the continuity equation, after neglecting all inductive terms, we arrive at the following equation:

$$\nabla\cdot\{[i\omega\epsilon+\sigma]\nabla\phi\}=0, \tag{2}$$

*Electronic address: boksiner@physics.rutgers.edu
†Electronic address: leath@physics.rutgers.edu

where ϕ is the electrostatic potential. The discretization of Eq. (2) on a square lattice leads to a lattice circuit of bonds where each bond comprises a parallel combination of a resistor and a capacitor. The capacitors are identical throughout the lattice, whereas the resistors vary to represent local conductivity [11,12].

We assume that the lattice consists of two types of bonds: those with initial (prebreakdown) resistance $\tilde{R}$ and capacitance $\tilde{C}$ and bonds with postbreakdown resistance $\tilde{R}_b$ and capacitance $\tilde{C}$. The breakdown of resistor $\tilde{R}$ occurs if the local field exceeds unity for a breakdown delay time $\tilde{T}_b$. The breakdown delay time $\tilde{T}_b$ represents the time it takes for a single element to fail. To reduce the number of independent parameters, we now formulate the problem in terms of dimensionless parameters.

B. Rescaling of parameters

In calculations, the relevant dimensionless parameter is the ratio of the postbreakdown to the prebreakdown element impedance. The bond impedance before breakdown is $(1/\tilde{R}+s\tilde{C})^{-1}=R(1+s\tilde{C}\tilde{R})^{-1}$ [13], the impedance after breakdown becomes $\tilde{R}_b(1+s\tilde{C}\tilde{R}_b)^{-1}$. Therefore, the ratio Γ of the postbreakdown to the prebreakdown bond impedance is given by

$$\Gamma=\frac{\tilde{R}_b(1+\tilde{s}\tilde{C}\tilde{R})}{\tilde{R}(1+\tilde{s}\tilde{C}\tilde{R}_b)}. \tag{3}$$

We note that s has units of $1/t$ and that $\tilde{C}\tilde{R}$ is a time constant of the lattice. So we use the following rescaling:

$$R_b=\frac{\tilde{R}_b}{\tilde{R}}, \tag{4a}$$

$$s=\tilde{s}\tilde{R}\tilde{C}, \tag{4b}$$

$$t=\frac{\tilde{t}}{\tilde{R}\tilde{C}}, \tag{4c}$$

and

$$T_b=\frac{\tilde{T}_b}{\tilde{R}\tilde{C}}. \tag{4d}$$

This rescaling leads to the form

$$\Gamma=\frac{R_b(1+s)}{(1+sR_b)}, \tag{5}$$

which corresponds to the impedance ratio for a circuit with unit resistance and capacitance before breakdown, as is illustrated in Fig. 1.

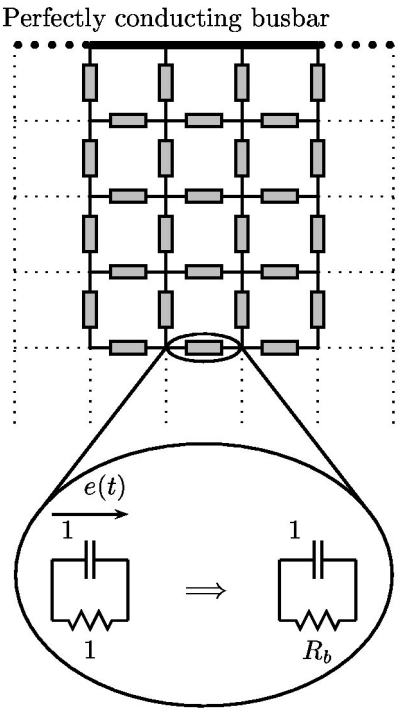

FIG. 1. A section of a semi-infinite lattice of resistors and capacitors. The resistors break down and their resistance changes from 1 to R_b if the local electric fields on a bond $e(t)$ exceeds unity for a time longer than the breakdown delay time T_b

1. Zero residual resistance

In the limit of zero residual resistance $\tilde{R}_b \to 0$, the limit of ratio Γ [in Eq. (3)] is zero. Since in this limit the capacitance is irrelevant, this is the same limit as the limit for $R_b \to 0$ in the quasistatic case ($\tilde{C}=0$) that we have discussed earlier [9].

2. Infinite initial resistance

An important special case is the limit of infinite initial resistance $\tilde{R} \to \infty$, which corresponds to breakdown in a media of infinite initial resistivity such as vacuum or an insulating gas. In the limit of infinite initial resistance $\tilde{R}$, the rescaling in Eq. (4) fails. So we apply the limit directly to Eq. (3) to obtain

$$\Gamma=\frac{\tilde{s}\tilde{C}\tilde{R}_b}{1+\tilde{s}\tilde{C}\tilde{R}_b}, \tag{6}$$

which we rescale using the residual time constant $\tilde{R}_b C$

$$s=\tilde{s}\tilde{R}_b\tilde{C}, \tag{7a}$$

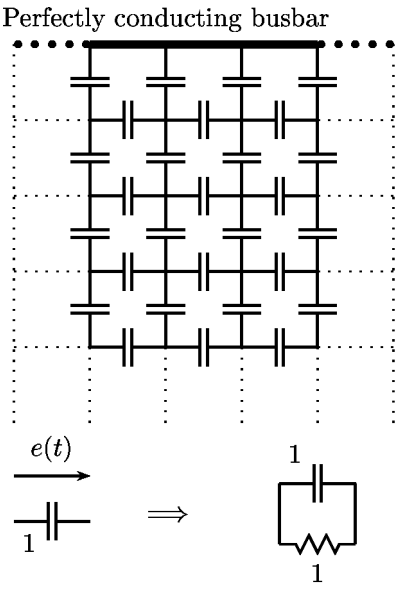

FIG. 2. A section of a semi-infinite lattice of capacitors corresponding to a medium with infinite initial resistivity. In this case, the capacitors break down and a resistance of 1 appears in series with the capacitor if the local electric fields on a bond $e(t)$ exceeds unity for a time longer than the breakdown delay time T_b

$$t=\frac{\tilde{t}}{\tilde{R}_b}\tilde{C}, \tag{7b}$$

and

$$T_b=\frac{\tilde{T}_b}{\tilde{R}_b\tilde{C}}. \tag{7c}$$

The rescaled quantities in Eq. (7) correspond to a circuit with unit capacitance and a breakdown resistance of unity as shown in Fig. 2.

In the quasistatic case, the ratio Γ is identical in the limits of zero residual resistivity and infinite initial resistivity. Thus, the two limits are equivalent for the quasistatic case. However, the introduction of time dependence breaks this symmetry leading to a different behavior for these two limiting cases.

C. Time scales

The effect of the rescaling in Sec. I B is to reduce the parameters of the lattice to dimensionless time scales. Thus, the case of infinite initial resistance has been parametrized by a single time scale T_b, the breakdown time delay. The case of finite initial resistance has been parametrized by two time scales, the breakdown time delay T_b and the time constant of the broken-down bond R_b. Note that although R_b is the rescaled residual resistance, it is also the rescaled time constant R_bC since $C=1$ after rescaling. The limit of zero residual resistance has no time scale and corresponds to an instantaneous evolution of the fields. In subsequent sections, we investigate the behavior of needle defects as a function of these time scales.

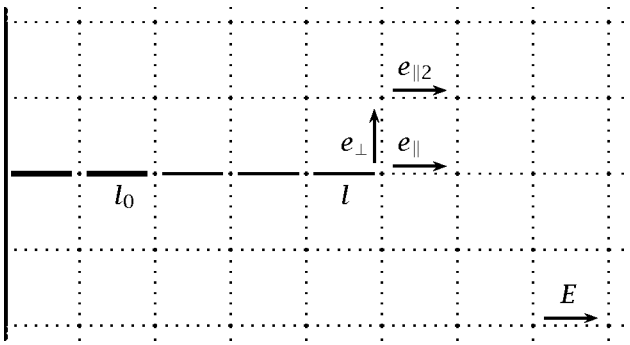

FIG. 3. An illustration of the parameters for a needle growing on a semi-infinite lattice with an infinitely conducting busbar. In this example, the needle has length $l=5$ and began with a needle defect of initial length $l_0=2$. The notations for the three fields $e_\parallel$, $e_\perp$, and $e_{\parallel 2}$ at the bonds near the needle tip that may break down next are shown.

II. GENERAL RESULTS FOR NEEDLE DEFECTS

We investigate the growth of a needle defect, consisting of a line of defect bonds, aligned along the direction of the applied field E in an otherwise homogeneous semi-infinite lattice. There are four independent parameters: the initial defect length l_0, the magnitude of the applied field E, the breakdown delay time T_b, and the residual resistance R_b of the defect bonds and subsequent broken bonds. Figure 3 illustrates the parameters for a needle propagating through a semi-infinite medium.

Our numerical simulation proceeds as follows. The initial needle of defect bonds along a vertical crystalline axis at the perfectly conducting busbar is prepared. A uniform electric field is applied to the lattice along the vertical crystalline axis. The field magnitude is determined by its value in a region far from the defects. The field increases adiabatically, that is, it varies very slowly in comparison to all other time constants of the system. During the entire breakdown process, the field magnitude varies infinitesimally.

All bonds where the local field exceeds the critical field, taken to be unity, for a critical delay time T_b break down, becoming defects and changing their resistance from 1 to R_b irreversibly. The local fields are then recalculated as a function of time for the new configuration of defects and the process is repeated.

We find that, depending on the parameters, the resulting needle growth exhibits a behavior that corresponds to one of the three phases of the breakdown process, namely, insulating, linear breakdown, or fractal breakdown, which we shall discuss. If the applied field is too small to initiate breakdown, the lattice remains in the insulating phase (there is no connected path of defects across the lattice). As the field increases, it reaches a critical value, which we shall call the initial breakdown field E_{bi}, which initiates the breakdown and causes the needle defect to start growing across the lattice. Subsequently, depending on the initial parameters, the

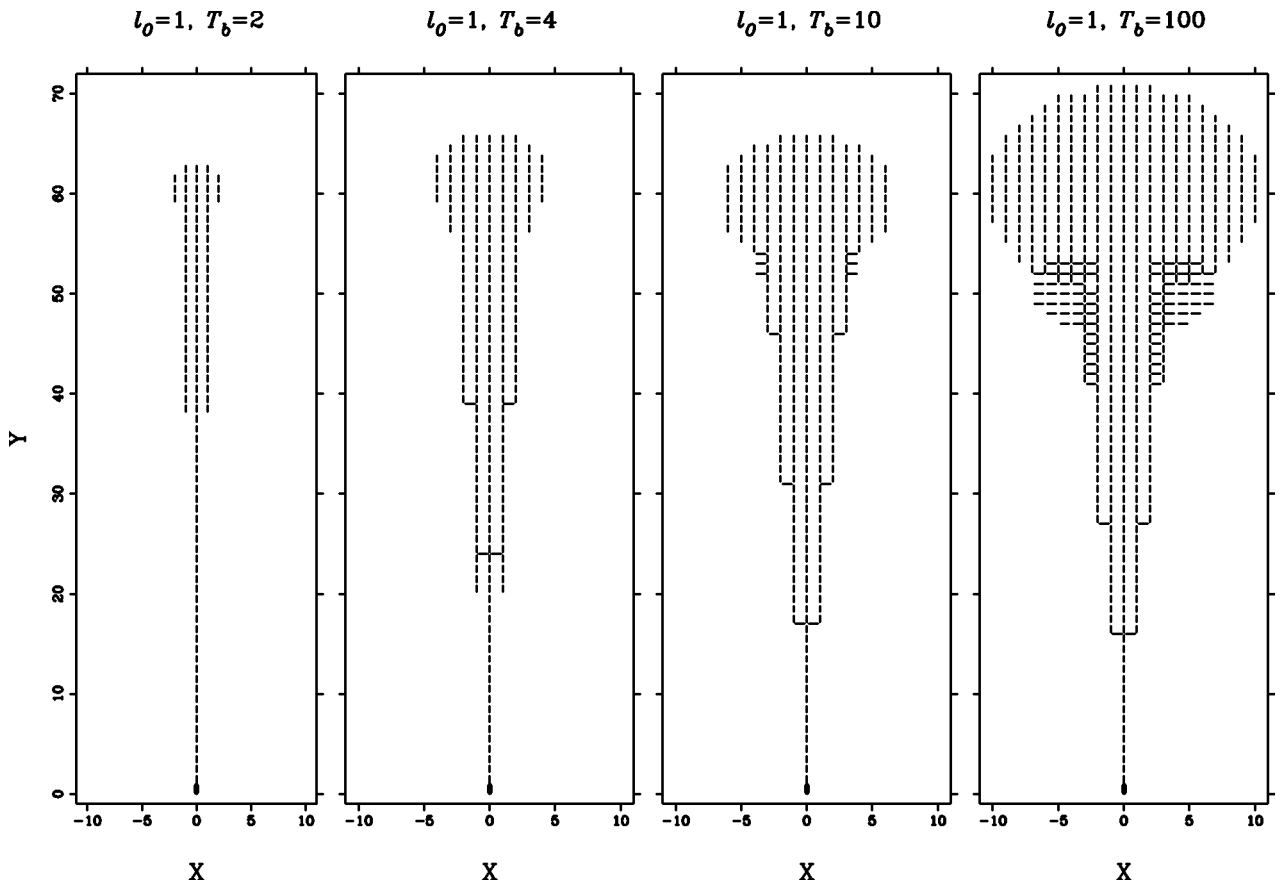

FIG. 4. Growth of breakdown clusters in vacuum for four different breakdown delay times T_b on a semi-infinite lattice with an initial defect of length $l_0=1$. The axes X and Y denote the number of lattice spaces in each direction. The breakdown path consists of bonds that break down at various times. For example, bonds in the Y direction generally break down before the nearby bonds in the X direction.

breakdown may grow linearly or with a fractal dimension. In addition, in some cases, oscillations in the breakdown process appear spontaneously. We discuss different phases and stages of breakdown in Sec. II B below.

A. Breakdown field

As the field is applied, the local field is generally the greatest at the tip of the needle (of length l_0) causing breakdown growth to begin there. This happens when $e_{\|}(E)=1$ for longer than T_b. In the time-dependent case, the breakdown field depends on how the field is applied. If the field is ramped up slowly in comparison to all other time constants of the lattice, then the breakdown field is the same as in the quasistatic case. In the quasistatic case, all transients have died out and the field distribution is determined by the analysis of the resistors only and is independent of capacitors. In this case, we previously found [9]

$$e_{\|} \approx E\left(1.132\sqrt{2l_0}+\frac{0.218}{\sqrt{2l_0}}\right), \tag{8a}$$

$$e_{\perp} \approx E\left(0.8\sqrt{2l_0}+\frac{0.6}{\sqrt{2l_0}}\right). \tag{8b}$$

Since the tip field increases as $\sqrt{l_0}$, the initial breakdown field E_{bi} approaches zero as $l_0^{-1/2}$. For needles of nonzero residual resistivity R_b, the tip fields saturates at a finite asymptotic value. In all cases, the tip field increases with needle length, so that once the needle begins to grow, it cannot stop, i.e., the system is brittle. Thus, the final breakdown field is equal to the initial breakdown field, i.e., $E_b = E_{\mathrm{bi}}$.

B. Breakdown path

We studied the path formed by the broken bonds. In the quasistatic case, the lattice can exist in three distinct states: insulating, linear breakdown, or fractal breakdown. We found a similar behavior in the time-dependent breakdown, although bifurcation into fractal breakdown is inhibited for smaller T_b and oscillations can appear in the breakdown process.

The needle begins to grow at $E=E_{\mathrm{bi}}$. At first, the growth consists of elongation of the needle so that the defect remains one dimensional (1D), but for defects with low residual resistivity, the needle bifurcates as it grows longer, growing fractally within a two-dimensional (2D) wedge. Figure 4 shows growth patterns for four different breakdown delay times T_b. The slope of the graph in Fig. 5 gives the fractal dimension D of the patterns using the procedure of

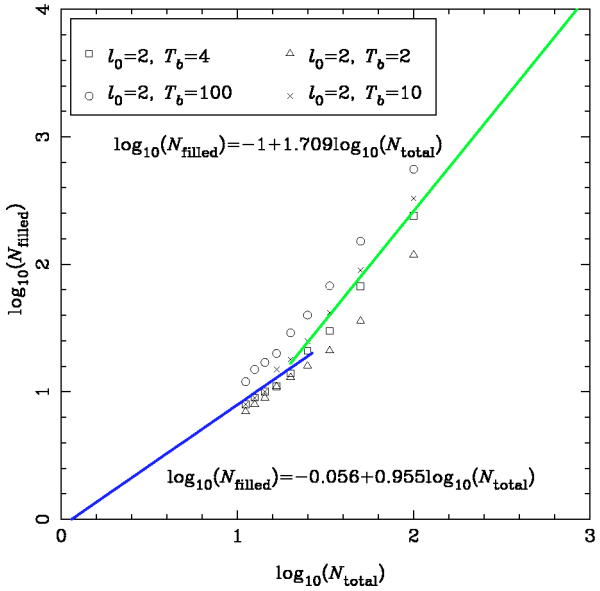

FIG. 5. Graph of the logarithm of the number of occupied boxes vs the logarithm of the total number of boxes covering a square area containing the breakdown cluster. l_0 is the size of the initial defect in units of lattice spacing. T_b is the breakdown delay time.

counting the number of filled boxes at various length scales [14,15]. The pattern starts linear but crosses over to fractal. Excluding finite lattice effects, the four patterns tend to exhibit a fractal dimension $D \simeq 1.71 \pm 0.03$. The fractal dimension in this case is consistent with that for the quasistatic case where $D \simeq 1.722 \pm 0.018$ [9].

As R_b increases or T_b decreases, the onset of the fractal (2D) growth occurs at longer needles and requires more iterations until, at a certain critical value of the residual resistance R_b and the breakdown delay time T_b, the growth remains purely one dimensional and the needle never bifurcates.

Although the breakdown paths for the quasistatic and time-dependent simulation are similar, there are several differences. In the time-dependent case, the fractal spreading does not start until a longer needle is realized. Also, the initial bifurcation for the time-dependent case involves vertical bonds only, whereas in the quasistatic case it involves the horizontal bonds. Note that Fig. 4 does not show the temporal order in which the bonds break down. The bifurcation begins with vertical bonds in all the clusters shown.

To understand the behavior of needle defects and the onset of bifurcation, we analyzed needle propagation to investigate the fields near the needle for various cases of initial and residual resistivity. Recall from Ref. [9] that propagation of the needle in the quasistatic case proceeds in a simple manner. The fields near the tip increase uniformly as the needle advances. As the tip fields increase, one or more bonds at the tip of the needle break down for each step. The number of bonds breaking down in each step increases uniformly. The tip fields and the number of bonds that break down in each step reach an asymptotic value for nonzero R_b or increase without limit in accordance with Eq. (8) for zero R_b.

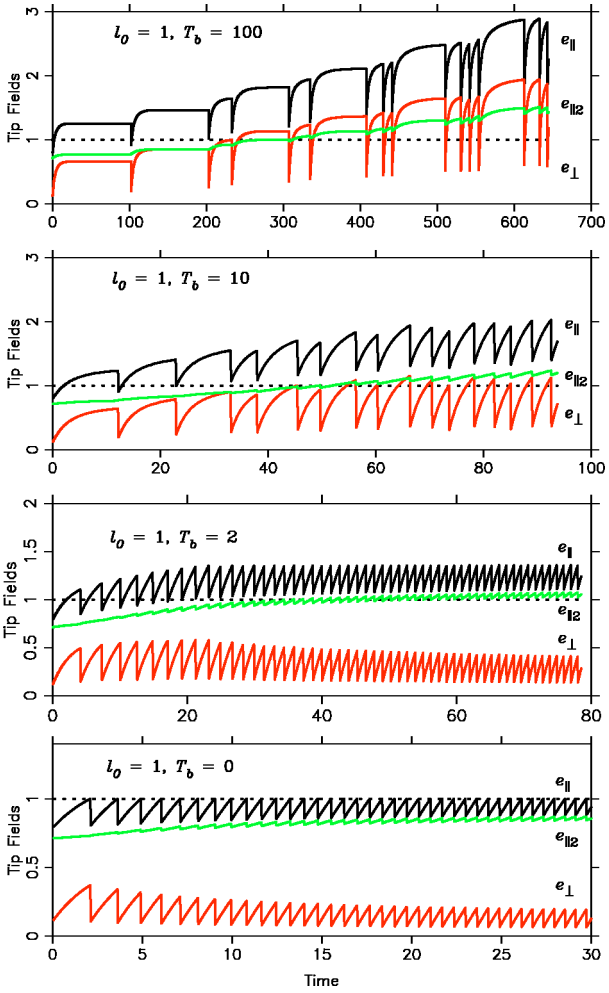

FIG. 6. The evolution of the tip fields of a needle as a function of time for various T_b and $l_0=1$. The time evolution is shown up to the time of bifurcation, except for $T_b=0$ where bifurcation does not occur.

However, in the time-dependent case investigated here, the needle propagation exhibits a complex behavior that defies such a simple description. We identified several phases of the propagation using a numerical simulation of the time evolution of the fields. We describe the results of numerical simulation of breakdown for lattices of infinite initial resistivity in Sec. III and the results for lattices of finite initial resistivity in Sec. IV. We describe the algorithm used to compute these fields in Appendix A 1.

III. RESULTS FOR LATTICES OF INFINITE INITIAL RESISTIVITY

The case of a lattice composed of bonds with infinite initial resistance (media with infinite initial resistivity) is an important practical case and also provides us with the understanding necessary for the case of nonzero initial resistivity. We assume that the applied field increases slowly in comparison to all time constants of the system. As the field reaches unity, breakdown of the first bond at the tip occurs after a breakdown delay time T_b. The field then builds up on the second bond. After the field reaches unity on this bond at

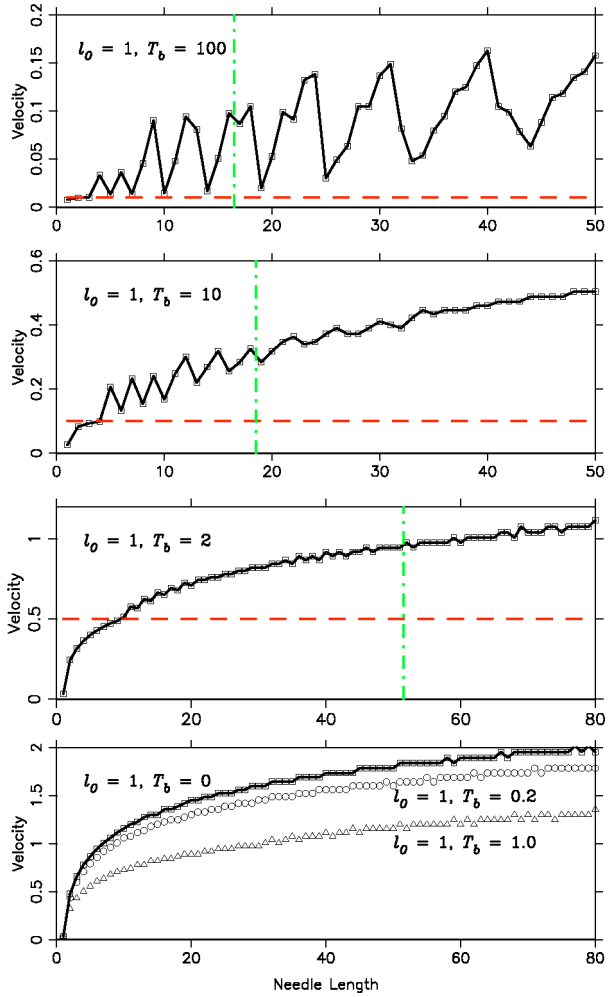

FIG. 7. The velocity of needle propagation, $1/t_s(l)$, as a function of needle length l for various breakdown delay times T_b and initial needle length $l_0=1$. The horizontal dashed line represents a velocity equal to $1/T_b$. The oscillations begin as this velocity is reached. The velocity plot extends beyond the point of bifurcation, but the bifurcation has been inhibited in this simulation in order to view the velocity of the propagating needle. The vertical dot-dashed line indicates where the onset of bifurcation would have been.

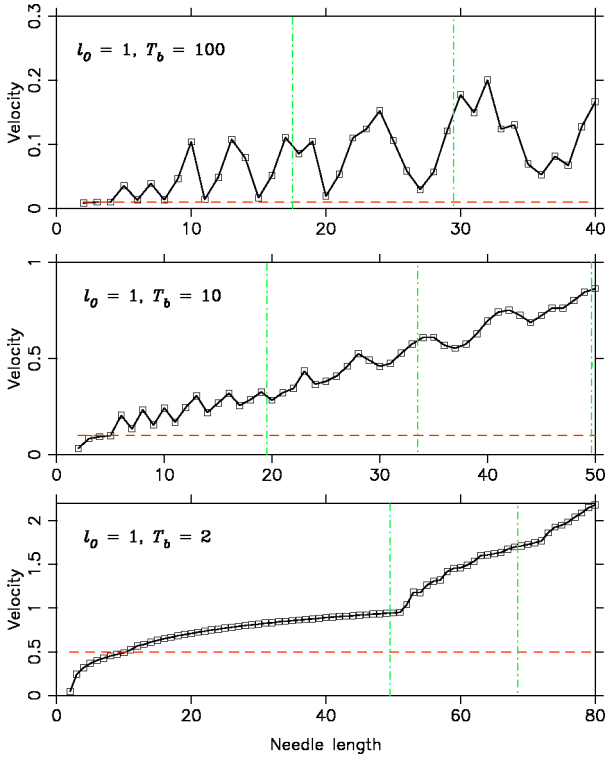

FIG. 8. The velocity of needle propagation, $1/t_s(l)$, as a function of needle length l for various breakdown delay times T_b and initial needle length $l_0=1$. The horizontal dashed line represents velocity equal to $1/T_b$. The oscillations begin as this velocity is reached. The needle is allowed to bifurcate. The vertical dot-dashed line indicates where the onset of bifurcation occurs and gives the subsequent sudden broadening to a wider breakdown wedge.

the tip, breakdown occurs again after breakdown delay T_b. This process continues as the needle grows. If the value of T_b is small, the field at the tip does not have time to increase much beyond unity. However, the velocity of propagation increases uniformly with needle length. If T_b is large, the fields can reach their quasistatic values. However, as the needle propagates, more and more charge gets transfered to the bonds further away from the needle. The fields at these bonds reach unity earlier, so that the delay for each step becomes smaller than T_b. At this point, the needle sprints through a section of the lattice. After several quick steps through the lattice, the charge transferred ahead of the needle is exhausted and a longer delay occurs. Thus, the velocity of needle propagation and the tip fields oscillate. We call this phase high velocity propagation with oscillations. As the needle propagates, the field $e_{\|2}$ can reach unity also and remain above unity sufficiently long to cause the needle to bifurcate. This initiates the ''fractal'' phase of needle growth.

Figure 6 shows several examples of the time evolution of the tip fields. Large fluctuations in the field appear after each breakdown as the needle advances and the observation bond where the tip fields are measured moves accordingly, causing a discontinuity in the tip field. The interval between the discontinuous jumps on the figure is the duration of each needle step which is the inverse of the velocity of needle propagation. We can see pronounced oscillations in the step durations and the terminal values of the tip field for each step at $T_b=100$ and less noticeable oscillations at $T_b=10$. Oscillations at $T_b=2$ occur also, but are not as obvious. Also, we see that the fields $e_{\|}$ and $e_{\perp}$ show a greater discontinuity compared to $e_{\|2}$. The reason is that $e_{\|}$ and $e_{\perp}$ receive their greatest charge contribution from the end bond, while $e_{\|2}$ receives a small contribution from the end bond, since it is almost parallel to the dipole charge on the end bond. This effect causes the bifurcation to be initiated entirely among bonds parallel to the direction of needle propagation. In the quasistatic case, bifurcation began at the perpendicular tip bonds. However, in the time-dependent case, the effect of breakdown of the end bond is to reverse the field on the perpendicular bond. This effect on $e_{\|2}$ is weak. Thus, $e_{\|2}$ can remain above unity longer as the needle propagates past a bond causing it to initiate the bifurcation.

Figures 7 and 8 show several examples of the needle ve-

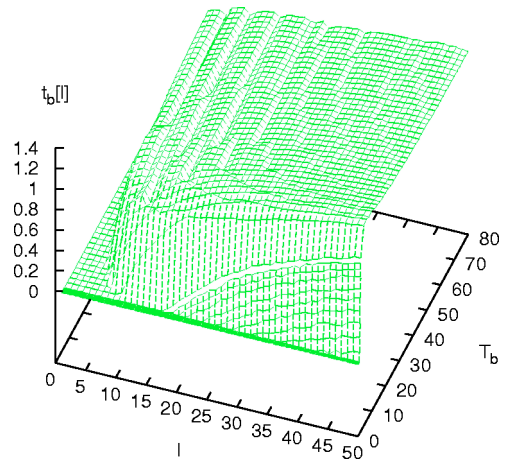

FIG. 9. The normalized time to breakdown, t_b, for a field at a bond parallel to the needle tip as a function of needle length l and breakdown delay time T_b for $l_0=1$. The corrugations are caused by oscillations.

locity as it propagates. We define needle velocity as an inverse of the time duration of each step t_s. Naively, we might expect that the velocity cannot exceed $1/T_b$, since a bond has to wait for this time before it can break down. However, we see that the velocity increases uniformly until it reaches $1/T_b$ (the dotted line). At this point, we can see the onset of high-velocity propagation and the velocity oscillations due to precharging effects. We observe that since the system is homogeneous, these oscillations arise from the intrinsic properties of needle propagation rather than from disorder in the system. Also, there is an increase in the period of oscillations at the point of bifurcation. There are no oscillations when there is no breakdown delay at $T_b=0$.

The approach of the needles to the bifurcation length can be expressed succinctly by considering a ''normalized time to breakdown,'' t_b, which is the ratio of the time a potentially bifurcating bond spends at a local field greater than unity $e_{\|2}\geqslant 1$ to the breakdown delay time. This quantity has

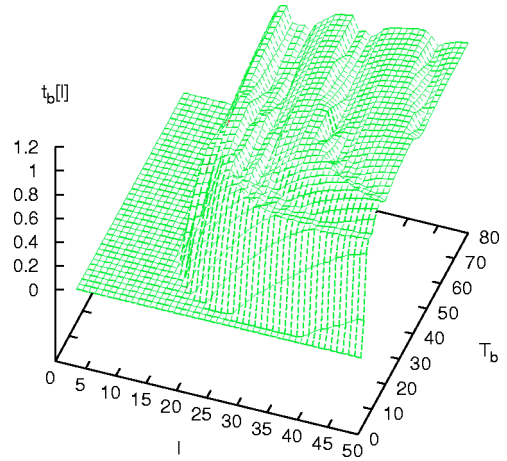

FIG. 10. The normalized time to breakdown, t_b, for a field at a bond parallel to the needle tip as a function of needle length l and breakdown delay time T_b for $l_0=3$. The corrugations are caused by oscillations.

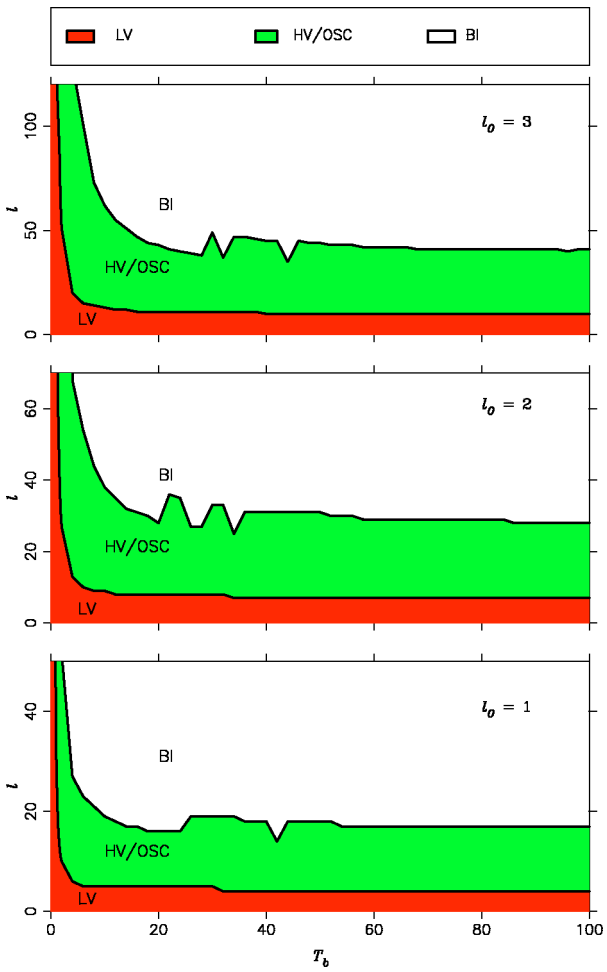

FIG. 11. The phase diagram of different phases of needle growth for three initial needle lengths. The phases are low-velocity needle propagation, high velocity with oscillations, and bifurcation.

the virtue that bifurcation occurs if this quantity reaches unity, analogous to the local electric field in the quasistatic case. The difference is that the quantity has a discontinuous derivative at zero due to the nonlinear nature of the underlying formula. The quantity becomes nonzero at a length consistent with our previous quasistatic results. Also, t_b experiences small oscillations as it increases due to the oscillations in time steps. These oscillations lead to oscillations in the bifurcation phase diagrams. Figures 9 and 10 show the t_b surface. The oscillations in t_b appear as corrugations in the surface.

Figure 11 shows the resulting phase diagram of needle propagation at the initial critical field. The three phases are clear, but the complexity and the richness of the needle propagation in the time-dependent problem is difficult to explain in simple terms. In the following section, we describe a simplified recursive map approximation that reproduces the essential qualitative behavior of the needle and allows us to understand the physical causes of this behavior.

Approximation using a recursive map

The complex behavior of the propagating needle in the time-dependent problem defies the very simple explanation

available for the quasistatic model. In this section, we provide a simplified model to help explain this behavior.

Our model uses a recursive map approximation (RMA) to evaluate the tip fields. This RMA uses the eigenvalue decomposition in Appendix A 1. To construct the RMA, we observe the weight of the ground state eigenvalue as the needle propagates. The ground state dominates if the needle propagates fast. The reason is that there is a limited time to discharge the needle bonds, so the charge is fairly uniform and similar to the ground state. If the breakdown delay time is very large and the needle propagates slowly, the charge dissipates completely at each step and appears as a δ function at the new tip bond after breakdown. We recall from the analysis of the eigenstates in Appendix A 1, that a δ-function wave packet decays approximately exponentially with time. In the intermediate propagation regime, the true needle state can be approximated as some mixture of a ground state and a δ-function at the tip.

Based on the foregoing observations, we constructed a summation using the results from the quasistatic case for the field enhancement multiplied by exponential decay factors. We use two decay factors, one for the ground state and one for the δ function at the tip. We use a simple expression to estimate the weight of the ground state and assign the rest of the charge to the δ function at the tip. This approximation qualitatively describes the effects we have seen in the simulations.

Using this decomposition, we construct the RMA as follows. Let us assume that we are interested in a tip field $e_{\|,l}(t)$ of a needle of length l from the moment the needle reaches this length until subsequent breakdown at this tip. Before the needle becomes l bonds long, it must progress through lengths l_0 through l. We will label each of these intermediate needle lengths by k, $l_0 \leqslant k \leqslant l$. The time interval between the breakdown that caused the needle to reach length k and the breakdown that causes the needle to reach length $k+1$ is T_k, i.e., the needle spends a time T_k at length k. The state of the needle of length k, at any time t, is described completely by the local electric field at each of its bonds that we will label by the index j, $1 \leqslant j \leqslant k$. For a lattice of capacitors, the local field is equal to the charge on the capacitor at the bond q_j, so we can write the full state of the needle of length k, using the bra-ket notation, as $|q_1 \cdots q_k\rangle(t)$.

The tip bond for a needle of length l is at position $(x,y) = (0,l+1)$. It does not have a significance as the tip bond though, until the needle reaches length l. As the needle propagates toward length l, this tip field $e_{0,l,\|}$ receives current and hence field contribution from each stage of the needle growth. In principle, the field can be expressed as a summation of contributions of each needle stage

$$e_{0,l+1,\|} = E_0 + \sum_{k=1}^{l} \mathcal{Z}[|q_1 \cdots q_k\rangle(t), l+1, t_k], \tag{9}$$

where $t_k = \Sigma_{p=1}^{k} T_p$, and $\mathcal{Z}$ is a numerically computable function relating a particular state of the needle $|q_1 \cdots q_k\rangle$ of length k to its field contribution at a bond at point $(0,l)$. If the function $\mathcal{Z}$ and the time evolution of the voltages of the needle state were known, it would be possible to solve for $e_{0,l+1}$ that becomes $e_{\|,l}(t)$ once $k=l$. Then we could find the time when this field has exceeded unity for a period greater than T_b, thus initiating the next breakdown and causing the needle to reach the length $l+1$. As the needle reaches the length $l+1$, the charge q_{l+1} is equal to the tip field $e_{\|,l}(t_{l+1})$. Thus, the complete state of the new needle of length $l+1$ is known from the state of the previous needle, just at the moment of breakdown and the value of the tip field. This can be expressed by a recursive map

$$\{|q_1 \cdots q_{l+1}\rangle(0), T_{l+1}\} \leftarrow \{|q_1 \cdots q_k\rangle(0), T_k\}_{k=1,\ldots,l}. \tag{10}$$

The recursive map in Eq. (10) can be evaluated exactly by expressing a needle state in orthogonal eigenfunctions. Appendix A describes an algorithm to compute the eigenfunctions and the electric-field enhancement function $\mathcal{Z}$. Another useful representation of each state is in terms of "δ-function" states where each state consists of a needle having a unit charge on bond k and zero charge elsewhere.

To complete our RMA, we assume that the needle state is a superposition of two nonorthogonal states. One state is a state of uniform charge distribution on a needle of length k denoted by $|k,0\rangle$, which approximates the lowest-order (ground) eigenstate. The other state is a state with a δ-function charge distribution at the tip denoted by $|k,1\rangle$, where the charge is unity at the tip and zero elsewhere.

The lowest-order state decays as $\exp(-\alpha_1 t)$ with α_1 given by Eq. (B3) and coefficients of Table I as $-1/\alpha_1(k) = 0.777 + 1.724k$. The tip δ-function state decays approximately as $\exp[-t^{u(k)}/\tau]$, with $\tau \approx 2.75$ and $u(k) \approx 0.8 + 0.2k^{-2}$ according to Fig. 24. As shown in the Appendix, if the charge decays exponentially from the needle, the field at any other bond increases exponentially proportional to $(1 - \exp[-\alpha_1(k)t])$ for state $|k,0\rangle$ and as $[1-\exp(-t^{u(k)}/\tau)]$ for state $|k,1\rangle$.

We can calculate the electric-field enhancement function $\mathcal{Z}$ for these two states from the analysis of the quasistatic cases reported in Ref. [9]. For both states, $\mathcal{Z}(|k,0\rangle, n)$ is

TABLE I. Coefficients for a linear approximation to time constants $-1/\alpha_p$ for the first ten eigenvalues.

p	a_p	b_p
1	0.777	1.724
2	0.433	0.457
3	0.446	0.261
4	0.489	0.180
5	0.535	0.136
6	0.578	0.108
7	0.618	0.089
8	0.655	0.075
9	0.689	0.065
10	0.720	0.056

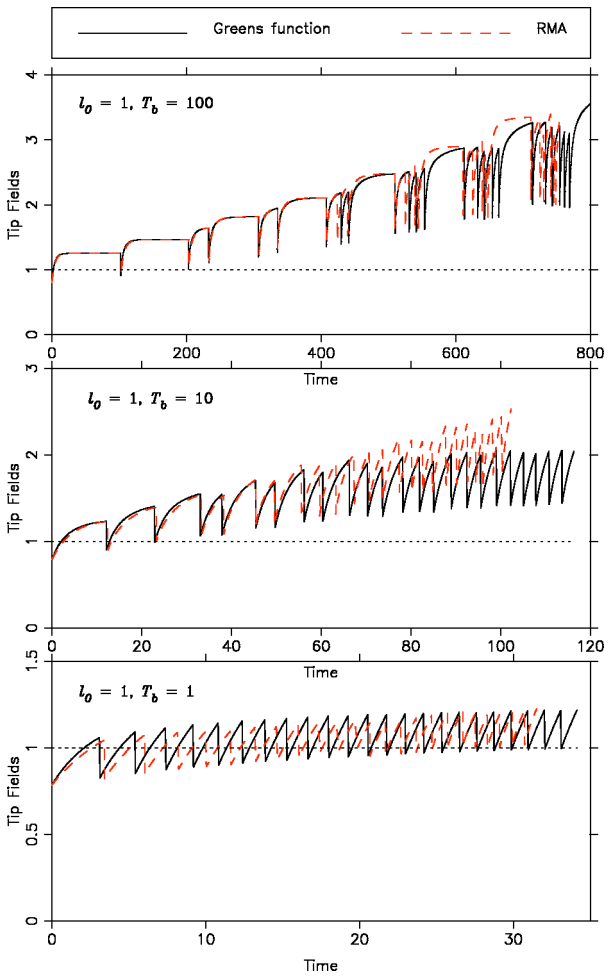

FIG. 12. A comparison of the tip field $e_{\|}(t)$ predicted by the calculation using the Green's function algorithm (solid lines) and the RMA (dashed lines) for three different delay times T_b and $l_0=1$.

simply the differential quasistatic field enhancement for a needle of length l on a resistive lattice. Thus, the field becomes

$$e_{0,l+1}(t)=E_0+\sum_{k=1}^{l} g_0(k)\mathcal{Z}(|k,0\rangle,l+1)\times\{1-\exp[-\alpha_1(t-t_k)]\}+\sum_{k=1}^{l} g_1(k)\mathcal{Z}(|k,1\rangle,l+1)\times\{1-\exp[-(t-t_k)/\tau]\}, \tag{11}$$

where g_0 and g_1 are the weights of the two states, respectively. We approximate the weights by an average of the charges over all bonds as follows:

$$x=\frac{[e_{\|,k-1}-e_{\|,k-2}\exp(-T_b/\tau)]}{e_{\|,k-1}}, \tag{12a}$$

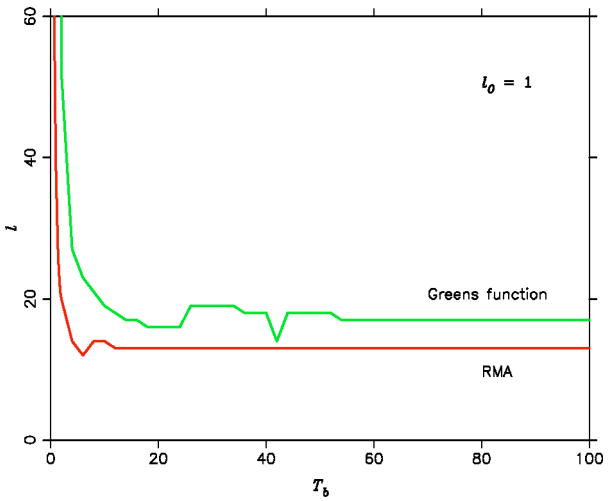

FIG. 13. A comparison of the onset of bifurcation as a function of T_b for $l_0=1$ as given by the calculation using the Green's function algorithm (upper curve) and the RMA (lower curve).

$$g_0=1-x+\frac{x}{k-1}, \tag{12b}$$

and

$$g_1=1-g_0. \tag{12c}$$

Figure 12 shows the comparison of the tip field between the simulation using the essentially exact calculation using the Green's function algorithm and the RMA. The figures show that the agreement is especially good at limiting values of T_b where the charge distribution is nearly uniform or nearly a δ function. The agreement is less good at intermediate values of T_b where other charge distributions contribute. The same calculation also predicts the other tip fields. Thus, the RMA predicts the onset of bifurcation as well as other complex needle behaviors. Figure 13 shows the comparison of the RMA against the Green's function simulation for calculation of the bifurcation phase diagram. There is a qualitative agreement, although there is a small difference in the bifurcation length.

IV. RESULTS FOR LATTICES OF FINITE INITIAL RESISTIVITY

We extend the results of Sec. III to the lattice model with bonds having a finite initial resistance shown in Fig. 1. We derive the Green's function algorithm in Appendix A 3, and show in the Appendix that the field evolves as in the case of infinite initial resistivity, except that the relevant time constants β_p are given by

$$\beta_p=\frac{\alpha_p(1-R_b)+R_b}{R_b}. \tag{13}$$

For small R_b, we have $\beta_p\approx\alpha_p/R_b$. In Fig. 14, we plot from the numerical simulations the time evolution of the tip

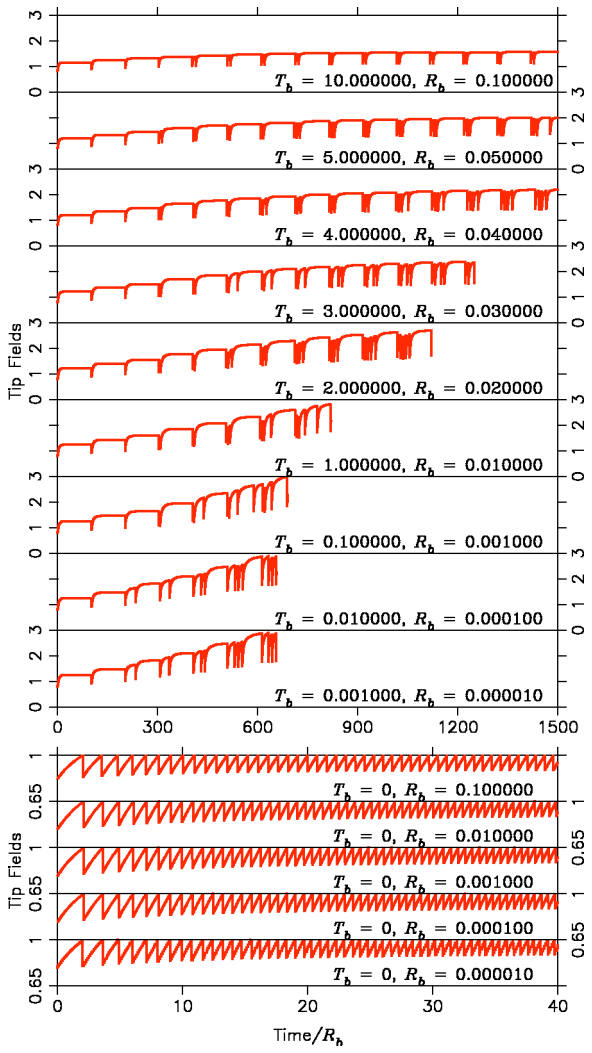

FIG. 14. The evolution of the parallel tip field $e_{\|}$ of a needle as a function of time for various R_b, for $T_b=0$ or $T_b=100R_b$, and for $l_0=1$ as given by the simulations. The time evolution is plotted up to the time of bifurcation, except for $T_b=0$ and $R_b \geqslant 0.04$ (top three curves) where bifurcation does not occur. The horizontal axis is the ratio of time to R_b.

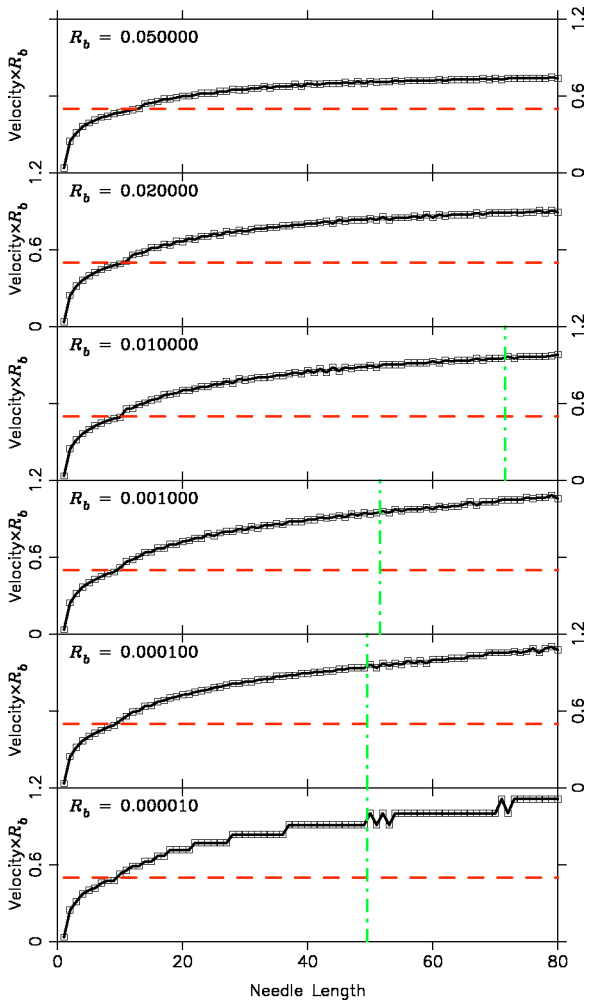

FIG. 15. The velocity of needle propagation, $1/t_s(l)$, as a function of needle length l for various residual resistances R_b at $T_b=2R_b$ and initial needle length $l_0=1$ from the simulations. The horizontal dashed line represents a velocity equal to $1/T_b$. The oscillations begin as this velocity is reached. The vertical dotted-dashed line indicates where the onset of bifurcation would have been. The velocity plot extends beyond the point of bifurcation, but the bifurcation has been inhibited in this simulation in order to view the velocity of the propagating needle.

fields at limiting values of $T_b=0$ and $T_b=100R_b$ for various R_b. The horizontal axis is the ratio of time over R_b. The scaling with R_b is seen in these graphs for small R_b. If we define $T_b'=T_b/R_b$ as $R_b'\to 0$, the system with a finite initial resistivity behaves like the system with infinite initial resistivity with an breakdown delay time T_b'.

As R_b increases, the quasistatic field enhancement decreases as described in Ref. [9]. This effect causes the scaling to fail because the charge ahead of the needle tip does not build up as quickly. Reference [9] shows that eventually the bifurcation is suppressed in the quasistatic case. A similar suppression of bifurcation occurs in the time-dependent case. We see from Fig. 14, which gives $e_{\|}$ vs time from the simulations, that the bifurcation length increases and then the bifurcation ceases to occur for the lengths studied. The oscillations remain, but become regular as the model settles into a limit cycle.

We can see the oscillations clearly by plotting the speed of the needle propagation as a function of needle length, as shown in Figs. 15–17.

As we did for infinite initial resistivity, we can construct phase diagrams for different T_b. Figure 18 shows phase diagrams for several R_b. We can see that while all cases exhibit oscillations, the bifurcation phase does not appear at sufficiently high R_b.

We studied the length l_{bi} that the needles reaches prior to the bifurcation for large T_b as a function of R_b for the first three initial needle lengths l_0. Figure 19 shows the results. This curve is similar to the curve of l_{bi} vs l_0 for the quasistatic case of Ref. [9]. However, the curve was based on bifurcation at the perpendicular adjacent bond. As we explained in Sec. III, the bifurcation in the time-dependent case occurs on the adjacent parallel bonds. Thus, we computed l_{bi}

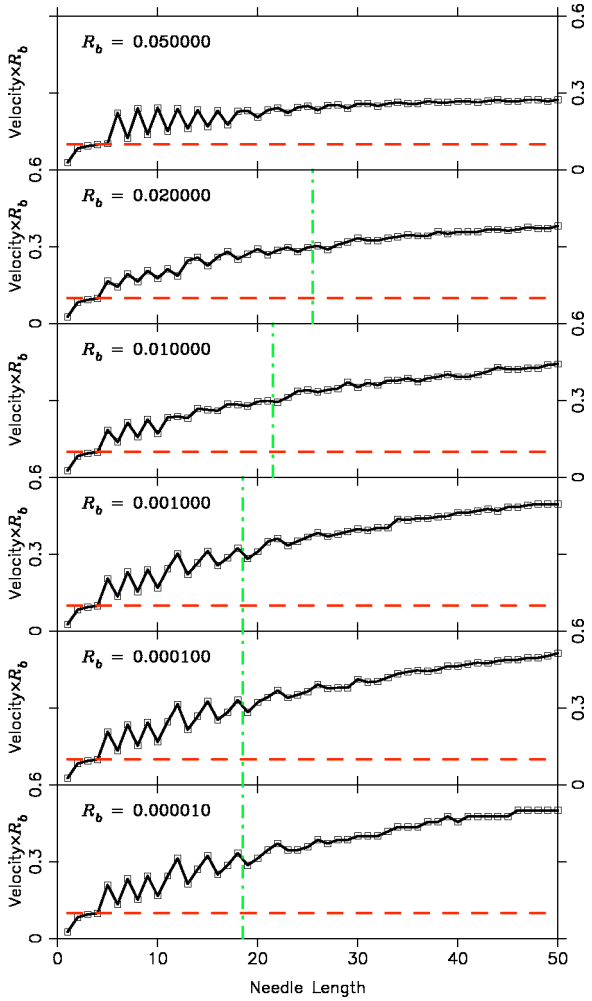

FIG. 16. The velocity of needle propagation, $1/t_s(l)$ as a function of needle length l for various residual resistances R_b at $T_b = 10R_b$ and initial needle length $l_0=1$. The horizontal dashed line represents a velocity equal to $1/T_b$. The oscillations begin as this velocity is reached. The vertical dot-dashed line indicates where the onset of bifurcation would have been. The velocity plot extends beyond the point of bifurcation, but the bifurcation has been inhibited in this simulation in order to view the velocity of the propagating needle.

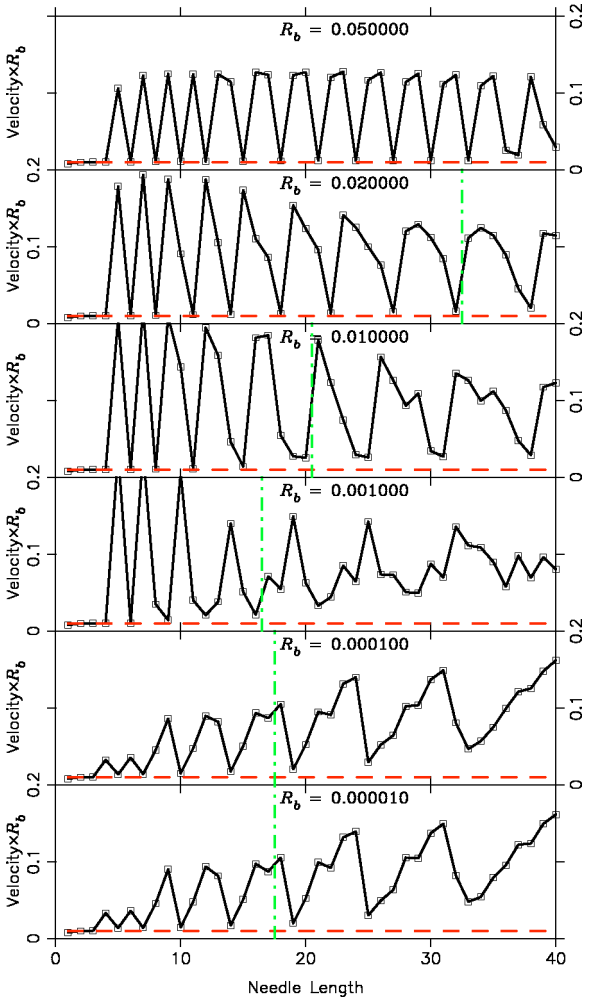

FIG. 17. The velocity of needle propagation, $1/t_s(l)$ as a function of needle length l for various residual resistances R_b at $T_b = 100R_b$ and initial needle length $l_0=1$. The horizontal dashed line represents a velocity equal to $1/T_b$. The oscillations begin as this velocity is reached. The vertical dot-dashed line indicates where the onset of bifurcation would have been. The velocity plot extends beyond the point of bifurcation, but the bifurcation has been inhibited in this simulation in order to view the velocity of the propagating needle.

vs R_b for the quasistatic case for bifurcation on the parallel bond. Figure 19 shows this result as well.

We observe that as R_b approaches a critical value $R_{\mathrm{bi}\infty}$, l_{bi} diverges for both quasistatic and time-dependent cases. We fit these data points to a power law of the form

$$l_{\mathrm{bi}} = (R_{\mathrm{bi}\infty} - R_b)^{-a}. \tag{14}$$

The quasistatic curves approach the critical values with exponent $a \approx 0.82 \pm 0.01$. The critical values $R_{\mathrm{bi}\infty}$ are 0.13, 0.06, and 0.039 for l_0 of 1, 2, and 3, respectively. The time-dependent points approach the critical values with exponent $a \approx 0.88 \pm 0.01$. The critical values $R_{\mathrm{bi}\infty}$ are ≈ 0.047, 0.023, and 0.015. Figure 19 shows these power-law lines also. The resulting fits are good in the limit of large T_b.

V. CONCLUSION

We investigated the time evolution and geometry of breakdown paths in time-dependent networks of capacitors and resistors under slowly increasing external fields. We investigated two classes of lattices, lattices with an elements with infinite initial resistance (purely capacitive lattices before breakdown) and lattices with elements having a finite initial resistance. For the lattices with infinite initial resistance, the speed of breakdown can be represented by a single time scale which we call the breakdown time delay. For lattices with both capacitors and resistors before breakdown, there are two relevant time scales, namely, the breakdown

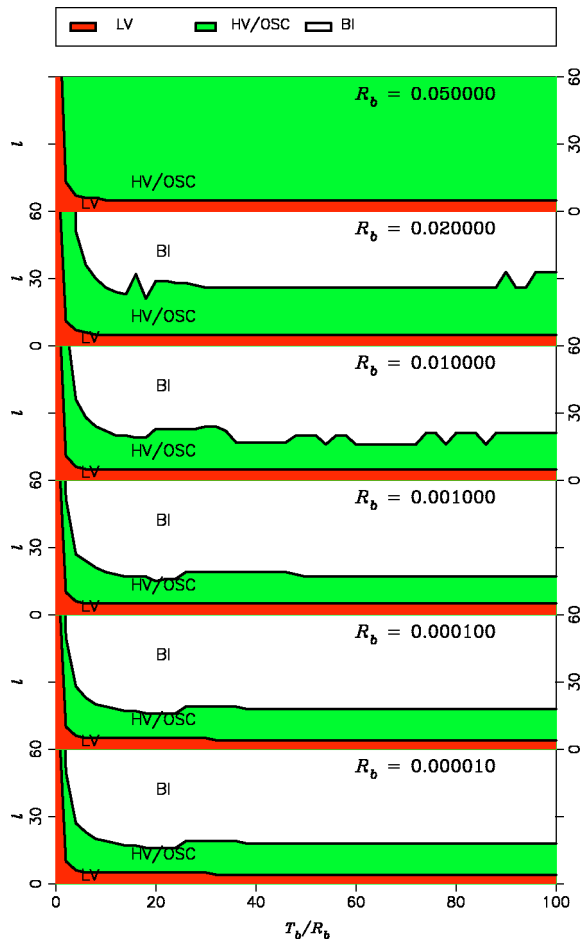

FIG. 18. The phase diagram of a different phase of needle growth for $l_0=1$ and several T_b. The phases are low velocity, high velocity with subsequent oscillations, and bifurcation.

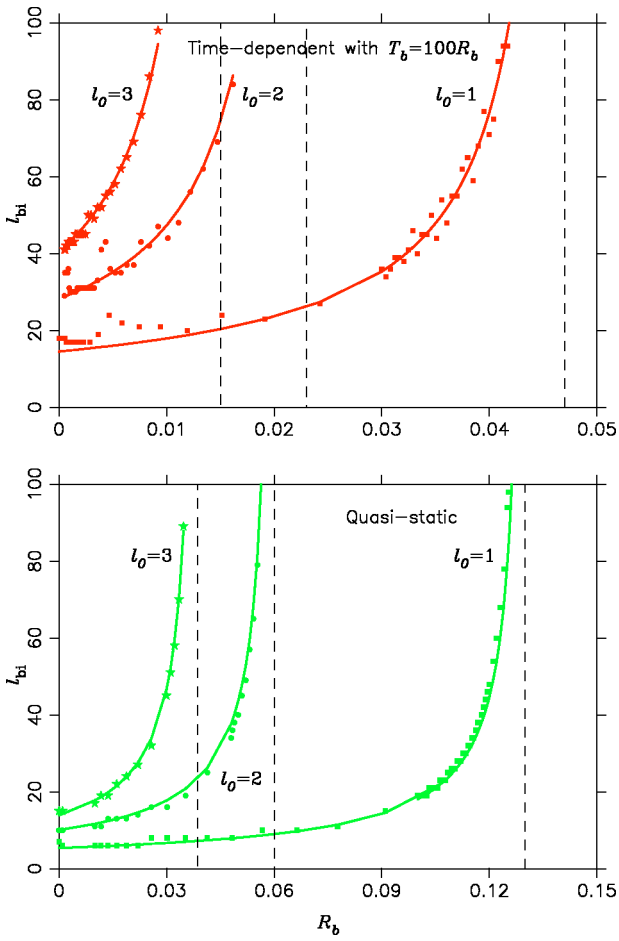

FIG. 19. Needle length at bifurcation l_{bi} as a function of R_b at three values of the initial needle length l_0 for a quasistatic case with bifurcation at an adjacent parallel bond (lower curve), and l_{bi} as a function of R_b for a time-dependent case at $T_b=100R_b$. The length l_0 and l_{bi} are in units of lattice spacing. The discrete points on the plot are from the simulations and the solid lines are power-law approximations with exponents of 0.82 ± 0.01 for the quasistatic case and 0.88 ± 0.01 for for the time-dependent case. The dashed lines are the critical values where $l_{\mathrm{bi}}\rightarrow\infty$ for each curve.

time delay and the time constant of the bond after breakdown.

We observe that if the local breakdown is slow compared to the evolution of the local field, there is a qualitative agreement with the results of the quasistatic case. If the local breakdown is rapid, the system never reaches the quasistatic situation.

Unlike the quasistatic case where the velocity of defect propagation increases monotonically with needle length due to the increase in the local tip field, the dynamical model indicates the onset of oscillations as fields build up and release. The oscillations that spontaneously occur are reminiscent of those that occur in the brittle fracture [16–18].

The behavior of this model is rich and there are several promising areas for further study. One such area is the incorporation of a more realistic model for variable time to breakdown as a function of local field-based physics of breakdown.

Another interesting possibility arises from the fact that a disordered lattice exhibits frequency-dependent conductivity even though all local properties are frequency independent [11]. Since the dielectric strength of the lattice depends on the amount of disorder, there is an intriguing possibility that dielectric strength of a material may be inferred in a nondestructive way from the frequency behavior of the material.

APPENDIX A: ALGORITHM

1. General formulation

We wish to calculate the electric field due to n defect bonds, labeled 1 through n, in an otherwise uniform, infinite, perfect square lattice. The basis for the algorithm used to calculate the time evolution of the fields is the algorithm that has been used previously to determine the field distribution for a resistive lattice with defects. The basis for both algorithms is the Green's function solution for the potential due to a constant unit current source into a site of an infinite square lattice of resistors. We show the development of the algorithm, repeating certain steps used to develop the earlier algorithm for the purely resistive lattice.

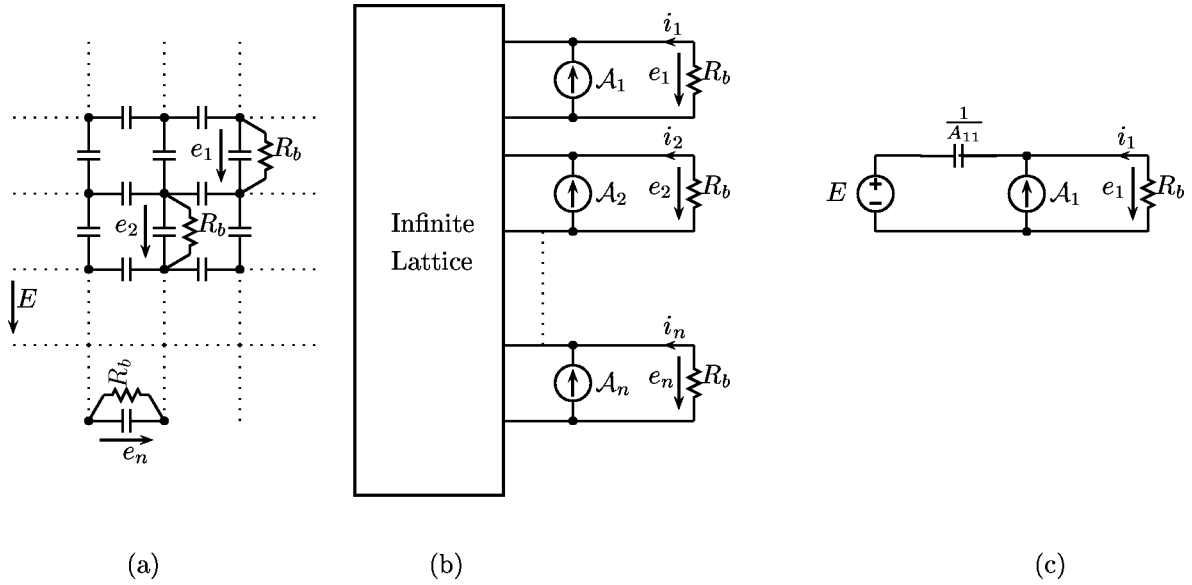

FIG. 20. The infinite lattice network of capacitors with n defect bonds (a), the equivalent n-port network (b), and an explicit representation of an equivalent single-port network (c).

The main consideration for the development of the algorithm is to treat the lattice in the frequency (Laplace-transform) domain. This allows us to view bonds as impedances and to manipulate them in a manner analogous to that used previously for the purely resistive lattice.

Consider the impedance of each defect bond. We can consider each defect impedance as comprising a parallel combination of the lattice impedance Z and an additional resistance selected so their parallel combination equals Z_b. Also, we can consider each nearest-neighbor node (site) pair of the perfect lattice as terminals of an arbitrary two-terminal linear passive electromagnetic system that can be represented by an equivalent linear electrical circuit. We call such pair of terminals a port. Thus, we can associate a port with each bond. As the lattice consists of resistors and capacitors that are linear in fields, the equivalent n-port circuit is linear in fields and obeys the superposition principle. If there are defects in the lattice, we represent them as resistors connected to the ports corresponding to the defect bonds. In addition, there are transients due to initial conditions across the capacitors. It is possible to represent an initial voltage $v(0^-)$ across a capacitor C in the Laplace domain as current sources of values $Cv(0^-)$ in parallel with the capacitor. Thus, we place a current source at each port of the equivalent circuit to represent the initial conditions. If the effect of transients and defects is represented by external elements, the open-circuit voltage at each port is equal to the applied field $\vec{E}(s)$ by symmetry. For a field applied along the vertical directions, the port voltage E_j is zero for a port at a horizontal bond and equal to $E(t)$ for a port corresponding to a vertical bond.

Thus, the voltage of an n-port circuit can be calculated by a linear superposition of voltages produced by the current into each port i_k with proportionality constant Z_{jk} and the open-circuit voltage at each port e_j,

$$e_j(s)=E_j(s)+\sum_{k=1}^{k=n}[i_k(s)+\mathcal{A}_k]Z_{jk}(s) \qquad \text{(A1)}$$

or in matrix form

$$\mathbf{e}(s)=\mathbf{E}(s)+[\mathbf{i}(s)+\boldsymbol{\mathcal{A}}]\overline{\mathbf{Z}}^{th}(s), \qquad \text{(A2)}$$

where $\boldsymbol{\mathcal{A}}$ is a vector of constants chosen to obtain the correct initial open-circuit voltage value.

In electrical-circuit theory, $E(s)$ and $Z(s)$ are known as Thévenin equivalent voltages and impedances. Also, Z_{jk} are called the driving-point and transfer impedances, they are equal to the voltage developed at port j when a unit current source is applied to port k.

The impedance can be found by calculating the voltage due to two unit current sources of opposite polarity attached at the nodes, namely, a dipole source. The solution for this impedance matrix for a lattice of unit resistors, which we call Watson's matrix, $\overline{\mathbf{A}}$, was developed in a previous work [9] based on the Green's function calculation of voltage due to a unit current source for a perfect square lattice network by Watson [19]. A calculation similar to that of Watson with a generalization to d d imensions has been shown in Ref. [20].

2. Formulation with infinite initial resistance

In the case of infinite initial resistance, the impedance of an unbroken bond is $1/s$. A parallel resistance $R_b=1$ is added to create breakdown. Impedances can be treated as resistances, and an equivalent circuit can be constructed for the lattice. Figure 20 shows the lattice and the equivalent n-port circuit. This figure also shows an example of a single-port circuit with explicit representation for the equivalent elements. The equivalent n-port circuit with the external current sources that represent initial conditions has the terminal voltage-current relationship given by

$$\mathbf{e}(s)=\mathbf{E}(s)+[\mathbf{i}(s)+\boldsymbol{\mathcal{A}}]\left(\frac{1}{s}\overline{\mathbf{A}}\right). \qquad \text{(A3)}$$

Solving for the current

$$s\mathbf{e}(s) = s\mathbf{E}(s) + [\mathbf{i}(s) + \boldsymbol{\mathcal{A}}]\overline{\mathbf{A}} \tag{A4}$$

or, equivalently,

$$\frac{d}{dt}\mathbf{e}(t) = \frac{d}{dt}\mathbf{E}(t) + [\mathbf{i}(t) + \boldsymbol{\mathcal{A}}\delta(t)]\overline{\mathbf{A}}, \tag{A5}$$

where $\delta(t)$ is the Dirac-delta function.

When breakdown occurs, a parallel resistance of unity appears in parallel with the port of the circuit. The voltage-current relationship for the resistance in the time domain is

$$\mathbf{e}(t) = -\mathbf{i}(t). \tag{A6}$$

Thus, we obtain an overall equation

$$-\frac{d}{dt}\mathbf{i}(t) = \frac{d}{dt}\mathbf{E}(t) + \overline{\mathbf{A}}[\mathbf{i}(t) + \boldsymbol{\mathcal{A}}\delta(t)]. \tag{A7}$$

The formal solution is

$$\begin{aligned}\mathbf{i}(t) &= -\exp(-\overline{\mathbf{A}}t)\int_{-\infty}^{t}\left[\frac{d}{dp}\mathbf{E}(p) + \boldsymbol{\mathcal{A}}\delta(p)\right]\exp(\overline{\mathbf{A}}p)\,dp \\ &= -\exp(-\overline{\mathbf{A}}t)\int_{-\infty}^{t}\frac{d}{dp}\mathbf{E}(p)\exp(\overline{\mathbf{A}}p)\,dp + \boldsymbol{\mathcal{A}}\exp(-\overline{\mathbf{A}}t).\end{aligned} \tag{A8}$$

We assume that breakdown occurs at $t=0$. Equation (A8) is valid for the circuit after breakdown only. This corresponds to viewing the field $\mathbf{E}(t)$ as being turned on at $t=0$. If the applied field is constant, the source terms become

$$\mathbf{E}(t) = \mathbf{E}U(t), \tag{A9a}$$

$$\frac{d}{dt}\mathbf{E}(t) = \mathbf{E}\delta(t), \tag{A9b}$$

where $U(t)$ is the Heaviside step function. Then, the solution becomes

$$\mathbf{i}(t) = \mathbf{E}\exp(-\overline{\mathbf{A}}t) + \boldsymbol{\mathcal{A}}\exp(-\overline{\mathbf{A}}t). \tag{A10}$$

If we let $\mathbf{i}_0$ be the vector of initial currents, we can express the solution as

$$\mathbf{i}(t) = \mathbf{i}_0\exp(-\overline{\mathbf{A}}t). \tag{A11}$$

This expression allows us to express the current evolution entirely in terms of the initial current, which is equal to the initial voltage across the bond. This compact expression is possible only for the network with an infinite initial resistance.

Again, the resulting current divides among the lattice elements just as in the resistive case. The field e (as well as the voltage) at the capacitor of bond k is the sum of the time integral of the current into the element i_k and the initial voltage into the element $e_k(0)$,

$$e_k(t) = \int_0^t i_k(t')\,dt' + e_k(0). \tag{A12}$$

At the moment of the first breakdown, the initial field is just the applied field so that $e_k(0) = E$.

We will label by a_{jk} the fraction of the current driven by source j into the bond k. The total current into a bond is a sum of contribution of the fraction for each defect, so the field is

$$e_k(t) = \sum_{j=1}^{n}\int_0^t a_{jk}i_j(t')\,dt' + e_k(0). \tag{A13}$$

We separate the field at each bond into the vector component of the applied field $E(t)$, and the enhancement field due to the defects in the lattice. The enhancement field is given by the summation over n defect bonds in Eq. (A13). This equation shows that the enhancement field is zero if the applied field is constant. Any enhancement results from the initial charge configuration and the time evolution of the applied field, for example, the adiabatic increase in the field to reach a constant value.

3. Formulation with finite initial resistance

Consider the impedance of a defect bond. We can consider it as a parallel combination of the lattice impedance Z and an effective resistance R', as shown in Fig. 21. The lattice impedance Z is a parallel combination of unit capacitance and unit resistance,

$$Z(s) = \frac{1}{1+s}. \tag{A14}$$

We select the effective resistance R' so that its parallel combination with unit resistance is R_b,

$$R' = \frac{R_b}{1-R_b}. \tag{A15}$$

Thus, the impedance matrix is given by $\overline{\mathbf{Z}}(s) = Z(s)\overline{\mathbf{A}} = \overline{\mathbf{A}}/(1+s)$.

We combine all the terms to obtain

$$\mathbf{e}(s) = \mathbf{E}(s) + [\mathbf{i}(s) + \boldsymbol{\mathcal{A}}]\left(\frac{1}{1+s}\overline{\mathbf{A}}\right). \tag{A16}$$

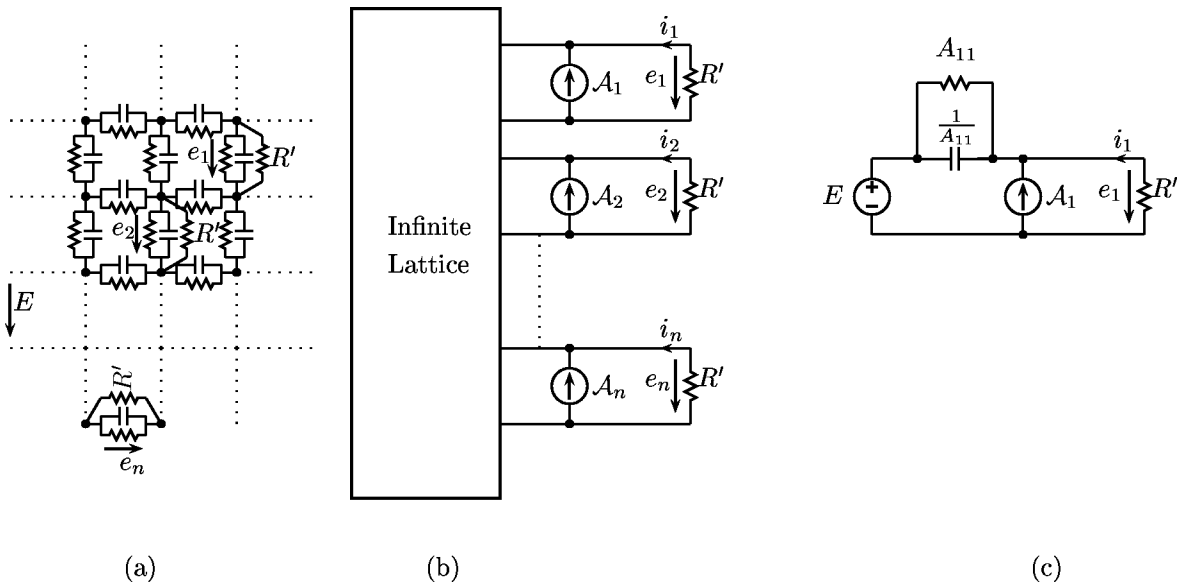

FIG. 21. The infinite lattice network of impedances with n defect bonds (a), the equivalent n-port network (b), and an explicit representation of an equivalent single-port network (c).

Solving for the current, we find

$$(1+s)\mathbf{e}(s)=(1+s)\mathbf{E}(s)+[\mathbf{i}(s)+\boldsymbol{\mathcal{A}}]\overline{\mathbf{A}}. \tag{A17}$$

We transform back to time domain to obtain the differential equation

$$\left(1+\frac{d}{dt}\right)\mathbf{e}(t)=\left(1+\frac{d}{dt}\right)\mathbf{E}(t)+[\mathbf{i}(t)+\boldsymbol{\mathcal{A}}\delta(t)]\overline{\mathbf{A}}. \tag{A18}$$

When breakdown occurs, a parallel impedance R' is attached to the port of the equivalent circuit. Its voltage-current relationship is given by Ohm's law

$$\mathbf{e}(t)=-R'\mathbf{i}(t). \tag{A19}$$

Thus, we obtain

$$-R'\frac{d}{dt}\mathbf{i}(t)=\left(1+\frac{d}{dt}\right)\mathbf{E}(t)+(\overline{\mathbf{A}}+R'\overline{\mathbf{I}})\mathbf{i}(t)+\overline{\mathbf{A}}\boldsymbol{\mathcal{A}}\delta(t). \tag{A20}$$

We define the matrix $\overline{\mathbf{B}}$ as

$$\overline{\mathbf{B}}=\frac{\overline{\mathbf{A}}+R'\overline{\mathbf{I}}}{R'}. \tag{A21}$$

Then, the equation for the current can be expressed as a matrix differential equation

$$-\frac{d}{dt}\mathbf{i}(t)=\frac{1}{R'}\left[\mathbf{E}(t)+\frac{d}{dt}\mathbf{E}(t)+\overline{\mathbf{A}}\boldsymbol{\mathcal{A}}\delta(t)\right]+\overline{\mathbf{B}}\mathbf{i}(t). \tag{A22}$$

We define $\boldsymbol{\mathcal{A}}'=(\overline{\mathbf{A}}/R')\boldsymbol{\mathcal{A}}$. Then, the formal solution for this system is

$$\mathbf{i}(t)=-\exp(-\overline{\mathbf{B}}t)\int_{-\infty}^{t}\exp(\overline{\mathbf{B}}p)\left[\mathbf{E}(p)+\frac{d}{dp}\mathbf{E}(p)\right]\frac{dp}{R'}+\boldsymbol{\mathcal{A}}'\exp(\overline{\mathbf{B}}t). \tag{A23}$$

We let $\mathbf{i}_0$ be the vector of initial conditions. In the special case that the applied field is constant, $\mathbf{E}(t)=U(t)\mathbf{E}$, the solution is

$$\mathbf{i}(t)=-(\overline{\mathbf{A}}+R'\overline{\mathbf{I}})^{-1}\left[\overline{\mathbf{I}}+\frac{\overline{\mathbf{A}}\exp(-\overline{\mathbf{B}}t)}{R'}\right]\mathbf{E}+\left(\frac{\mathbf{E}}{R'}-\mathbf{i}_0\right)\exp(\overline{\mathbf{B}}t). \tag{A24}$$

We note that the initial current i_0 is equal to the open-circuit voltage at the time of breakdown $\mathbf{e}^{oc}(0)$ divided by the additional resistance R'. The open-circuit voltage cannot change discontinuously because it is a voltage across a capacitor, while the current through the additional resistors can jump abruptly. We can simplify Eq. (A24) to obtain

$$\mathbf{i}(t)=-[\overline{\mathbf{I}}-\exp(-\overline{\mathbf{B}}t)](\overline{\mathbf{A}}+R'\overline{\mathbf{I}})^{-1}\mathbf{E}-\frac{e^{oc}(0)}{R'}\exp(\overline{\mathbf{B}}t). \tag{A25}$$

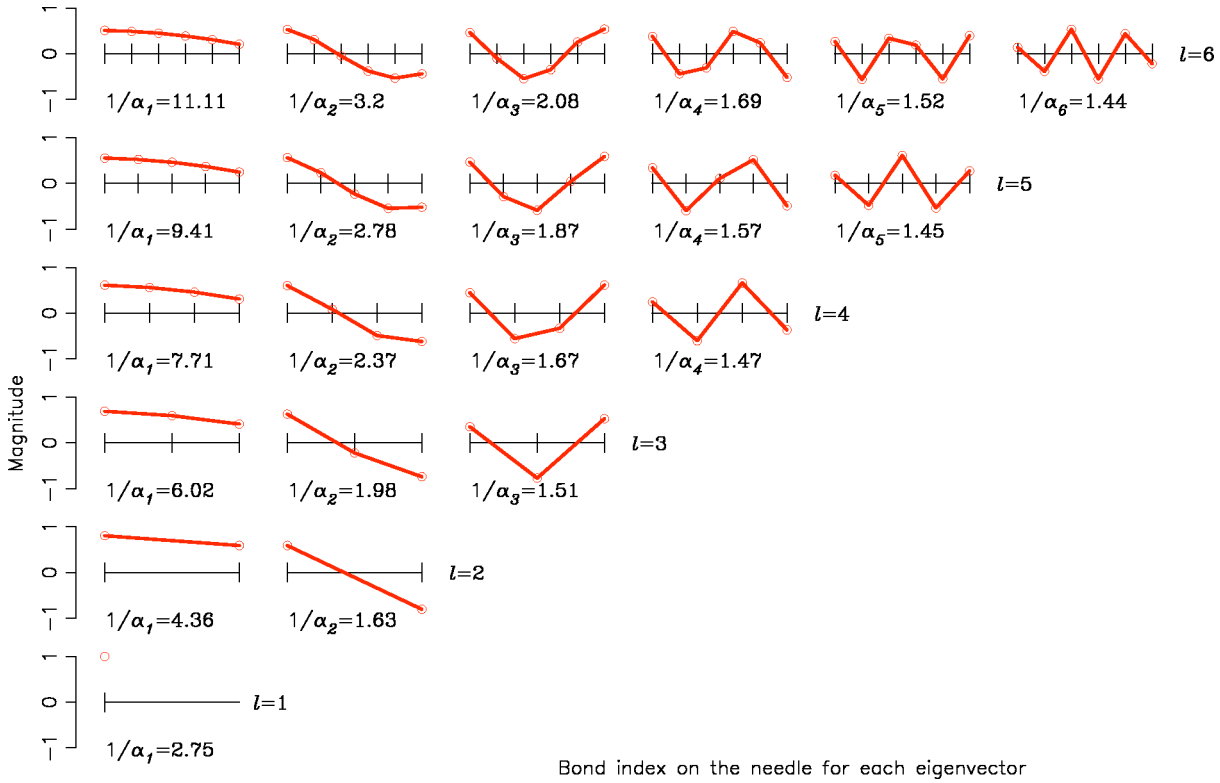

FIG. 22. Eigenvectors $|n,p\rangle$ and their associated time constants $1/\alpha_p$ for needles of up to six bonds.

This expression has the expected form of a sum of a steady-state solution that is identical to the solution obtained for the resistive case [9], a transient solution, and a decaying term due to initial conditions.

The resulting current divides among the lattice elements just as in the resistive case. The local field is the voltage across each resistor, which is equal to the current through each resistor.

The differential equation for each circuit element is

$$e(t)+\frac{d}{dt}e(t)=i(t), \tag{A26}$$

where $e(t)$ is the field across the bond. Its transform is

$$e(s)=i(s)\frac{1}{1+s}+\frac{1}{1+s}e_0. \tag{A27}$$

Thus, the solution for the node voltage becomes

$$e=E(t)+\int_0^t i(t')\exp(-t+t')dt'+[e_0-E(0)]\exp(-t). \tag{A28}$$

APPENDIX B: THE STRUCTURE OF TIME-DEPENDENT SOLUTIONS FOR A NEEDLE DEFECT

Understanding the fields arising from a needle is important for understanding the initiation of breakdown. We derived expressions for time-dependent solutions in Appendixes A 1 and A 2. These expressions involve exponentiation of matrices and can be evaluated by various techniques. One approach that provides considerable insight into the nature of the solution is the eigenvalue decomposition.

1. Infinite initial resistance

First, we look at the solution with infinite initial resistance. The numerical procedure for calculating Watson's matrix $\overline{\mathbf{A}}$ is given in Ref. [9]. To understand the behavior of the solution, we express the initial state of fields across each needle bond $|n\rangle(t=0)$, where n is the needle length, as a sum of eigenvectors $|n,p\rangle$ of $\overline{\mathbf{A}}$, where $p=1,\ldots,n$. Note that the field across a bond is a state variable, i.e., it cannot change instantaneously. Each eigenvector has a corresponding eigenvalue $-\alpha_p$. The initial current across each bond is equal to the initial voltage and the initial charge, since both the capacitance and parallel resistance are equal to unity. Thus, we can consider each eigenvalue as belonging to a state with a lifetime $1/\alpha_p$.

Once the eigenvalues are determined, the time evolution of charges on the needle depends on the initial conditions and their decomposition into the eigenvectors. Let C_p be the weight $C_p=\langle n,p|n\rangle(t=0)$ of each eigenvector $|n,p\rangle$ in a particular initial state $|n\rangle(t=0)$. Then Eq. (A11) decomposes as

$$\mathbf{i}(t)=|n\rangle(t)=\sum_{p=1}^{n} C_p|n,p\rangle\exp(-\alpha_p t). \tag{B1}$$

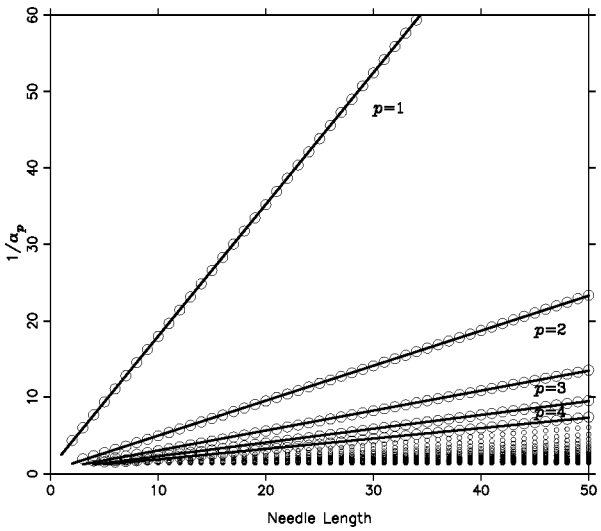

FIG. 23. Time constants $1/\alpha_p$ for eigenvalues of a given order vs needle length.

The final result for the enhancement field becomes

$$e_k(t)=\sum_{j=1}^{n}\int_{-\infty}^{t}a_{jk}\sum_{p=1}^{n}C_p x_{pj}\exp(-\alpha_p t')dt'$$

$$=\sum_{j=1}^{n}\sum_{p=1}^{n}\frac{1-\exp(-\alpha_p t)}{\alpha_p}a_{jk}C_p x_{pj}, \qquad \text{(B2)}$$

where x_{pj} is the element j of the eigenvector $|n,p\rangle$. Note that parameters in this equation can be calculated from Watson's coefficients for the resistive lattice.

The eigenvectors $|n,p\rangle$ can be arranged in the order of decreasing eigenvalues or, equivalently, in the order of increasing time constant $1/\alpha_p$. Figure 22 shows the set of complete eigenvalues and eigenvectors for short needles. The most symmetrical longest wavelength eigenvectors have the largest time constant. Figure 23 shows the dependence of the time constant on the needle length. The plot shows that the time constant is linearly proportional to the needle length l:

$$1/\alpha_p(l)=a_p+b_p l. \qquad \text{(B3)}$$

Table I shows the values of these coefficients for the first ten eigenvalues.

Dependence on the initial conditions

The coefficients C_p depend on initial conditions. Two important limiting cases are a uniform initial charge distribution or a δ function distribution where the last bond has unit charge and all other charges are zero. We consider the δ function distribution in detail.

The tip fields produced by the δ functions can be computed by expanding the δ function in terms of the eigenvectors and computing the resulting field dependence. Figure 24 shows the time dependence of the field for the increasing needle length. We try to approximate this behavior as

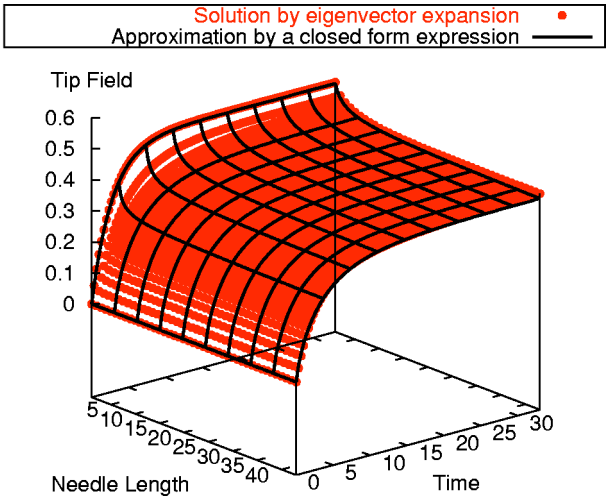

FIG. 24. The time evolution of the tip field $e_\parallel$ for a needle of length $1\geqslant l\geqslant 43$ with an initial charge of unity on the last bond and no charge on the remainder of the needle (δ-function response). The discrete points represent the calculation using the expansion in eigenvectors computed with the Green's function algorithm [Eq. (B2)]. The surface hatched with solid lines is the closed-form approximation (Eq. (B4)].

$v(l)[1-\exp(-t^{u(l)}/\tau)]$. The coefficient $v(l)$ is the asymptotic field enhancement. It is equal to the value obtained for the quasistatic case for a single defect on a semi-infinite lattice. Thus, it takes on its largest value 0.5 for $l=1$ and approaches 0.36 for large l. The time constant τ is 2.75 for $l=1$ from our calculations of eigenvectors with results shown in Fig. 22. We notice that as l increases, the time variation of the tip field flattens. This is likely due to the asymptotic behavior of the eigenvalues for long needles that are likely to dominate the behavior of δ functions. The deviation from exponential behavior is likely due to a few long-lived low-order states. We approximate this as a power law in the exponent as $u(l)\approx 0.8+0.2l^{-2}$, with the exponent dependence obtained from a curve fit. The resulting approximation in the form of

$$e_\parallel=\left(0.36+\frac{0.14}{\sqrt{l}}\right)\times\left\{1-\exp\left[-\frac{t^{(0.8+0.2/l^2)}}{2.75}\right]\right\} \qquad \text{(B4)}$$

fits the calculated values well as can be seen in Fig. 24.

2. Nonzero residual resistivity

The solution for nonzero residual resistivity, given in Eq. (A25), consists of a homogeneous part that is identical to the solution for the resistive case, and a transient part that has a form similar to that for a time-dependent case of the zero residual resistivity. If we focus on the transient part, we can apply the eigenvalue decomposition as we did in Appendix . We attempt to use properties of the matrix $\mathbf{A}$ to illuminate the properties of the matrix $\mathbf{B}$.

We recall that $\mathbf{B}=(\mathbf{A}+R'\mathbf{I})/R'$. We label eigenvalues of $\mathbf{B}$ by β_p and the corresponding eigenvectors by $|n,p\rangle$ with the dependence on R_b implicit. From the definition of eigen-

values $\overline{\mathbf{B}}-\beta\overline{\mathbf{I}}=0$, we see that $\alpha_p=R'+\beta_pR'$, so that

$$\beta_p=\frac{\alpha_p+R'}{R'}. \tag{B5}$$

The eigenvectors corresponding to each eigenvalue are the same as for the case of infinite initial resistivity.

We determine the time evolution as in the case of infinite initial resistivity. We note that the state $(\overline{\mathbf{A}}+R'\overline{\mathbf{I}})^{-1}\mathbf{E}$ is the state as t approaches ∞, which is also a solution of the quasistatic (purely resistive) case. We label this state by $|n\rangle(\infty)$. Equation (A25) decomposes as

$$\mathbf{i}(t)=\sum_{p=1}^{n} D_p|n,p\rangle[1-\exp(-\beta_pt)] + \sum_{p=1}^{n} C_p|n,p\rangle\exp(-\beta_pt), \tag{B6}$$

where the coefficients are $C_p=\langle n,p|n\rangle(0)$, and $D_p=\langle n,p|n\rangle(\infty)$. The final result for the enhancement field becomes

$$e_k(t)=e_k(0)\exp(-t) + \sum_{j=1}^{n}\sum_{p=1}^{n} a_{jk}C_px_{pj}\frac{\exp(-t)-\exp(-\beta_pt)}{\beta_p-1} + \sum_{j=1}^{n}\sum_{p=1}^{n} a_{jk}D_px_{pj}\left[1+\frac{\exp(-\beta_pt)-\beta_p\exp(-t)}{\beta_p-1}\right], \tag{B7}$$

where x_{pj} is the element j of the eigenvector $|n,p\rangle$. Again, parameters in this equation can be calculated from Watson's coefficients for the resistive lattice. Also, this equation shows that all transient fields decay eventually leaving only the steady-state solution (resistive lattice).

In the limiting case of zero residual resistivity, $\beta_p\to\infty$ so that the enhancement field becomes

$$e_k(t)=e^{oc}(t)+e_k(0)\exp(-t)-\sum_{j=1}^{n} a_{jk} \times(\langle n,j|\overline{\mathbf{A}}^{-1}\mathbf{e}^{oc}|n,j\rangle)[1-\exp(-t)]. \tag{B8}$$

[1] L.A. Dissado, J. Phys. D: Appl. Phys. **23**, 1582 (1990).
[2] P.M. Duxbury, P.D. Beale, and P.L. Leath, Phys. Rev. Lett. **57**, 1052 (1986).
[3] P.M. Duxbury, P.L. Leath, and P.D. Beale, Phys. Rev. B **36**, 367 (1987).
[4] Y.S. Li and P.M. Duxbury, Phys. Rev. B **36**, 5411 (1987).
[5] Y.S. Li and P.M. Duxbury, Phys. Rev. B **38**, 9257 (1988).
[6] S.S. Manna and B.K. Chakrabarti, Phys. Rev. B **36**, 4078 (1987).
[7] L. Benguigui, Phys. Rev. B **38**, 7211 (1988).
[8] H. Takayasu, Phys. Rev. Lett. **54**, 1099 (1985).
[9] J. Boksiner and P.L. Leath, Phys. Rev. E **57**, 3531 (1998).
[10] M. Sahimi, Phys. Rep. **306**, 213 (1998).
[11] J.C. Dyre and T.B. Schroder, Rev. Mod. Phys. **72**, 873 (2000).
[12] J.C. Dyre, Phys. Rev. B **48**, 12 511 (1993).
[13] A. Papoulis, *Circuits and Systems: A Modern Approach* (International Thomson, New York, 1997).
[14] D. Stauffer and A. Aharony, *Introduction to Percolation Theory* (Taylor & Francis, London, 1994).
[15] H. Peitgen, H. Jurgens, and D. Saupe, *Chaos and Fractals* (Springer-Verlag, New York, 1992).
[16] F.F. Abraham, D. Brodbeck, R.A. Rafey, and W.E. Rudge, Phys. Rev. Lett. **73**, 272 (1994).
[17] T. Cramer, A. Wanner, and P. Gumbsch, Phys. Rev. Lett. **85**, 788 (2000).
[18] D. Holland and M. Marder, Phys. Rev. Lett. **80**, 746 (1998).
[19] B. Watson, Ph.D. thesis, Rutgers University, 1975.
[20] G.D. Jozsef Cserti and A. Piroth, Am. J. Phys. **70**, 153 (2002).